Published in final edited form as:
Mol Cancer Res. 2013 August ; 11(8): 845–855. doi:10.1158/1541-7786.MCR-13-0032.

Suppression of ser/thr phosphatase 4 (PP4C/PPP4C) mimics a novel post-mitotic action of fostriecin, producing mitotic slippage followed by tetraploid cell death

Benjamin Theobald[1,*], **Kathy Bonness**[1,*], **Alla Musiyenko**[1], **Joel F. Andrews**[1,2], **Gudrun Urban**[1], **Xizhong Huang**[1], **Nicholas M. Dean**[3], and **Richard E. Honkanen**[1,2,†]

[1]Department of Biochemistry and Molecular Biology, University of South Alabama College of Medicine, Mobile, Alabama 36688

[2]Mitchell Cancer Research Institute, University of South Alabama College of Medicine, Mobile, Alabama 36688

[3]Department of Pharmacology, ISIS Pharmaceuticals, Carlsbad, California 92010

Abstract

Fostriecin is a natural product purified from *Sterptomyces* extracts with antitumor activity sufficient to warrant human clinical trials. Unfortunately, difficulties associated with supply and stable drug formulation stalled further development. At a molecular level, fostriecin is known to act as a catalytic inhibitor of four PPP-family-phosphatases, and reports describing the syntheses of designed molecules in the class suggest derivatives targeting enzymes within the fostriecin sensitive sub-family can be produced. However, it is not clear if the tumor selective cytotoxicity of fostriecin results from the inhibition of a specific phosphatase, multiple phosphatases, or a limited subset of fostriecin sensitive phosphatases. How the inhibition of sensitive phosphatases contributes to tumor selective cytotoxicity is also not clear. Here, high-content time-lapse imaging of live cells reveals novel insight into the cellular actions of fostriecin, showing that fostriecin induced apoptosis is not simply induced following a sustained mitotic arrest. Rather, apoptosis occurs in an apparent second interphase produced when tetraploid cells undergo mitotic slippage. Comparison of the actions of fostriecin and antisense-oligonucleotides specifically targeting human fostriecin-sensitive phosphatases revealed that the suppression PP4C alone is sufficient to mimic many actions of fostriecin. Importantly, antisense-oligonucleotides targeting PP4C induce apoptosis, with death occurring in tetraploid cells produced following mitotic slippage. This affect was not observed following the suppression of PP1C, PP2AC or PP5C. Although future studies are needed to clarify how the suppression of PP4C triggers mitotic slippage/apoptosis, our observations suggest further development of fostriecin class inhibitors should consider PP4C as a potentially important target.

Keywords

fostriecin; protein phosphatase; PP4C; serine; threonine; mitosis

[†]Please address correspondence to: Professor Richard E. Honkanen, Department of Biochemistry and Molecular Biology, MSB 2362, University of South Alabama, Mobile, AL 36688, Phone: 251 460-6859, fax 251 460-6850, rhonkanen@southalabama.edu.
[*]Indicates equal contribution of these two authors

Introduction

Fostriecin and structurally related phosphate monoesters produced by *Streptomyces* sp. (i.e. cytostatin) display cytotoxicity and antitumor activity [for rev see (1, 2)]. Cytostatin has potent cytotoxic activity towards melanoma and leukemia cell lines and inhibits B16 melanoma lung metastasis in a mouse model of cancer progression (3). The antitumor activity of fostriecin (also called PD-110,161, CI-920 or NSC-339638) has been evaluated extensively [(4); for review see (1, 5)]. Fostriecin demonstrates potent cytotoxicity against a number of cancer cell lines and marked antitumor activity in animals [for review see (1, 5, 6)]. To evaluate its potential for use as a novel antitumor agent in humans, fostriecin entered human clinical trials (7, 8). Although limited, the data obtained from the Phase I trials indicate plasma levels of fostriecin associated with antitumor activity in animals (9) can be achieved in humans (7, 8). Unfortunately further development has been suspended for nearly a decade, due to early controversies regarding its mechanism of action, problems associated with the supply of fostriecin from natural sources, and difficulty associated with stable drug formulation (8).

Now methods for synthesis are known, and the molecular targets of fostriecin are becoming clear. Fostriecin (1, 10–13), structurally related natural products [e.g. cytostatin (14, 15) phospholine, leustroducsin, and phoslactomycins (1, 16, 17)] and designed analogs used to explore the structure-function properties and mechanisms of action of molecules in the class (11, 12, 15), all inhibit the catalytic activity of a subset of PPP-family serine/threonine protein phosphatases. Fostriecin is a potent inhibitor of PP2AC [IC_{50} ~0.2 nM; (10, 11, 13)], a strong inhibitor of PP4C [IC_{50}~4 nM; (18)], and a weak inhibitor of PP1C and PP5C (IC_{50} 72 and 60 μM respectively) (10, 11). Structural studies have revealed that the fostriecin sensitive phosphatases share a common catalytic mechanism (19). Structure activity relationship (SAR) studies indicate selectivity for PP2AC is derived from the interaction of C3 with a non-catalytic cysteine of PP2AC (C^{269}), which is contained in the β12-β13 loop that resides adjacent to the highly conserved catalytic pocket (11, 12). This cysteine is not conserved in PP1C or PP5 (12, 19), and the predicted covalent adduct with PP2AC has been shown using a biotin-labeled derivative (20). The β12-β13 loops of PP4 and PP6 contain a homologous cysteine, suggesting it servers as a commonality for strong inhibition (11, 12, 19). However, to our knowledge these predicted actions on PP4C and PP6C have not been tested experimentally. Fostriecin has no apparent affects on PP2B (calcineurin), PP7 or PPM-family phosphatases [for review see (1, 6)]. SAR studies have also provided insight into other features needed for potency, selectivity, and stability, sparking renewed interest in the development of compounds in this class (11, 12, 15, 21, 22).

The basis for the antitumor activity of fostriecin is not clear. At the cellular level, fostriecin enters cells via folic acid transporters (23, 24), and at concentrations sufficient to inhibit PP1C, PP2AC, PP4C and PP5C (>125 μM) it kills both tumor and normal cells (13). Many of the toxic effects are cell cycle independent and similar to the toxic actions produced by other natural compounds that act as strong, nonselective inhibitors of PP1C, PP2AC, PP4C, and PP5 (e.g. microcystin-LR and calyculin A). Nonetheless, similar to early observations made with paclitaxel (taxol), preclinical studies indicate that fostriecin has antitumor activity in animals at non-toxic concentrations (≤50 μM) (5, 8, 9, 25). At ≤50 μM fostriecin induces an apoptotic response in many types of cancer cells (26). However, fostriecin induced apoptosis is slow, requiring >24–48 hours, and death is preceded by the accumulation of cells with 4N-DNA (13, 27, 28). Cantharidin, a less selective natural inhibitor of PP1-PP5 that also has cytotoxic and antitumor activity, produces a similar accumulation of cells with 4N-DNA prior to the onset of apoptosis. This suggested the antitumor activity of both compounds could arise from their ability to prolong mitosis, triggering mitotic/spindle checkpoint control mechanisms (29).

To help clarify the relationship between tumor-selective cytotoxicity and phosphatase inhibition we developed 2′-*O*-methyl phosphorothioate deoxyoligonucleotides capable of specifically suppressing the expression of fostriecin-sensitive phosphatases (29–31). Previous studies have shown that, like fostriecin, the suppression of PP2ACα, but not PP2ACβ, PP1Cγ1 or PP5C, induces a prolonged mitotic-arrest (29). Further investigations revealed that PP2AC forms a complex with a kinetochore-associated protein (Sgo1/MEI-S332) during metaphase (32–35). The PP2AC/Sgo1/kinetochore complex protects cohesin residing at the kinetochore from phosphorylation-mediated dissociation prior to the onset of anaphase (32–35). Thus, when PP2AC is suppressed, the activation of mitotic kinases (i.e. Plk1, Aurora A/B) results in the premature dissociation of sister chromatids. This prevents biorientation (the attachment of duplicated chromatids via their kinetochores to opposite poles within a microtubule-based mitotic spindle), which activates or maintains the spindle-assembly check-point controls that prevent progression into anaphase (32–35). These observations lead to the widely accepted hypothesis that fostriecin induced apoptosis was simply due to it ability to produce a prolonged mitotic arrest via the inhibition of PP2AC. However, the prolonged mitotic arrest induced by the suppression of PP2AC alone did not trigger apoptosis (29), prompting us to re-examine the actions of fostriecin. Here, high-content time-lapse imaging of live cells reveals that fostriecin induced apoptosis is not simply produced by the induction of a prolonged mitosis. Rather, death occurred in tetraploid cells produced following mitotic slippage. This effect was mimicked by antisense targeting PP4C (but not by antisense targeting PP1C, PP2AC, or PP5C), revealing a novel role for PP4C during mitotic progression.

Materials and Methods

Cell Culture

A549 and HeLa cells were obtained from ATCC. A well characterized stable HeLa-cell line constitutively expressing a histone 2B-GFP fusion protein (H2B-GFP; HeLa-H2B-GFP cells) was a generous gift from Dr. Kevin Sullivan (36). Both cell lines were cultured in DMEM (Dulbecco's Modified Eagle's Medium) supplemented with 10% Fetal Bovine Serum (FBS) and L-Glutamine (4.0 mM) at 37° C in 5% CO_2.

Chemicals

Fostriecin was synthesized as described previously (11).

Oligonucleotide synthesis and assay for oligonucleotide inhibition of PP2ACα or PP4C expression

Phosphorothioate deoxyoligonucleotides and 2′-O-methyl phosphorothioate deoxyoligonucleotides were synthesized and purified as described previously (37). The indicated cells were plated in 60 mm dished and cultured in DMEM containing 10% FBS. When ~50% confluent, the cells were treated with oligonucleotides as previously described (30, 38). Because phosphorothioate oligonucleotides act through RNAase H-dependent mRNA cleavage mechanism in cells, the ability of each oligonucleotide to specifically inhibit the expression of PP4C was initially determined by northern blot analysis probing for levels of PP4C mRNA (39). Antisense oligonucleotides targeting PP1C (γ1), both isoforms of PP2Ac (PP2ACα, PP2ACβ) and PP5 have been developed and characterized previously (29–31, 40). The characterization of antisense oligonucleotides targeting PP4C is provided as supplemental material (Figure 1S).

Immunoblotting of PP2A, PP4C, PP5 and PP6

Western analysis was performed as described previously using polyclonal rabbit antibodies generated against a synthetic 15 amino acid peptide identical to unique regions of PP2A, PP4C, PP5 and PP6 (29–31, 41). The antibody targeting PP2A does not discriminate between PP2Aα and PP2Aβ (29).

Caspase 3 activity

Caspase 3 activity was measured using a CASP3C colorimetric assay (optical density at 405 nm) according to the instructions provided by the manufacture (Sigma). All experiments were repeated at least three times.

Flow cytometry

A549 Cells were harvested, stained with propidium iodide (PI) and DNA content flow cytometry was performed as described previously(29).

Live cell imaging and time-lapse video microscopy

HeLa-H2B-GFP cells were cultured in 60-mm dishes and incubated at 37°C in 5% CO_2 using a Neuve-live cell chamber fitted into an Eclipse Nikon TE 2000-U microscope (Nikon Instruments Inc. Melville, NY). Image acquisition was achieved using a COOLSNAP ES monochrome camera and processed using Elements (Nikon) and MetaMorph Premier software (Universal Imaging, Downingtown, PA).

Analysis of live cell imaging—To study mitotic progression we employed live cell imaging in combination with time-lapse video microscopy using an established HeLa cell line (HeLa-H2B-GFP) expressing histone-2B fused with green fluorescent protein (29, 32, 36). Here, both fluorescent and differential interference contrast (DIC) images of live cell cultures were taken at timed intervals (every 2–5 minutes) for the duration of experiments lasting from 12 to 72 hours. Short exposure times and neutral density filters were used to minimize UV exposure to cells, and control experiments using solvent or mismatched antisense oligonucleotides were conducted to ensure the observations made were not due to UV-damage produced during fluorescent imaging. In each experiment images of >300 cells can be analyzed at every time point for the duration of the experiment. H2B-GFP expression in interphase cells is dispersed throughout the nucleus, and chromosome condensation (marking the onset of prophase) is easily distinguished from dispersed nuclear fluorescence of interphase cells (Figure 1A). Metaphase alignment of sister chromatids, mitotic defects, and sister chromatid separation (indicating the onset of anaphase) can also be easily distinguished. The nuclear envelope breakdown and the onset of cytokinesis are easily detected in corresponding DIC images. Therefore, analysis of sequential images allows for quantitative assessment of the time needed for cell cycle progression from prophase to metaphase, anaphase, and cytokinesis. Analysis of live cell images also allows us to provide a detailed description of mitotic defects induced by the various treatments, and to quantitate the frequency that these defects are produced.

Results

Quantitation of cell cycle progression in controls—To further characterize the cellular effects of fostriecin, live cell imaging, in combination with time-lapse video microscopy was employed using a HeLa cell line that stably expresses histone-2B fused with green fluorescent protein (HeLa-H2B-GFP). This stable cell line is widely used because it allows high-resolution imaging of chromosomes without compromising nuclear or chromosomal structures (29, 32, 36), and it has proven useful as a powerful tool to study

agents that affect chromosome condensation, metaphase plate alignment of sister chromatids, and mitotic progression into anaphase (29, 32, 36). In each experiment, images of ~300–500 live cells were taken at timed intervals (generally every 5 minutes) for 24–72 hours, as indicated. Individual images were then examined and analyzed with the aid of advanced imaging software (Elements® and Metamorph®). This procedure allows us to simultaneously assess several aspects of cell cycle progression in ~50–300 individual cells/experiment. Then, following the fate of each cell, the duration required for progression from nuclear envelope break down (NEBD) to: 1) chromosome alignment at the metaphase plate, 2) the onset of anaphase, 3) chromosome decondensation, 4) cleavage furrow formation, and 5) cytokinesis was quantified. When abnormal behaviors were observed, the time of onset (relative to NEBD) and the ensuing fate of the cells were noted.

Progression through mitosis in control cells is illustrated in Figure 1A. The data shown is typical of cell populations for >10 experiments, in which 50–100 mitotic cells are analyzed in each experiment. Quantitation of the data revealed that in untreated or solvent treated controls progression from NEBD (designated as 0 min) to chromosome decondensation and cytokinesis requires 1.3 +/− 0.82 (mean +/− SD; n=300) hours (Figure 2A). During this time, chromosome alignment at the metaphase plate (indicted with an asterisk) is observed ~20 min after NEBD in >97 % +/− 3 (mean +/− SD) of the cells scored (n=500). Separation of sister chromatids, indicating the onset of anaphase, occurs 49 min +/− 25 minutes thereafter (Mean +/− SD; n=300) and is not observed until all of the chromosomes are aligned. In 96 % of the cells analyzed, chromosome decondensation and cytokinesis occur <2.5 hours after the onset of NEBD. A delay during mitosis (defined as cells with condensed chromosomes that fail to proceed into anaphase in <2.5 hours) is rarely observed in untreated or solvent controls (<4%, n=300) and is therefore considered an indication of “mitotic arrest”.

Fostriecin prolongs mitosis and prevents cytokinesis—Fostriecin is known to induce apoptosis, and previous studies using FACS-analysis have shown that prior to death fostriecin produces a dose-dependent accumulation of cells with 4N-DNA (27). Consistent with previous studies, in the HeLa-H2B-GFP model fostriecin (<50 μM) produced no notable effects on cell cycle progression prior to NEBD (Figure 1B; designated as 0 min). Following chromosome condensation fostriecin prevents the proper alignment of sister chromatids at the metaphase plate (indicated at 45 min and 4.6 hr by arrows). Cells that do not achieve metaphase alignment arrest and do not progress into anaphase. Dose-response studies revealed a concentration-dependent increase in the frequency of cells with aberrant metaphase alignment, with maximal efficacy achieved with 50 μM fostriecin (Figure 1D). Quantitation of the data revealed that fostriecin prolongs mitosis [(5.4 hr +/− 0.25; mean +/− SE); compare red bars shown in Figure 2 A with Figure 2 B; Figure 2E]. During this period, the arrested cells remain rounded in appearance and the chromosomes remain condensed. The sister chromatids that do align at the metaphase plate do not separate, and the chromosomes that fail to align move in an unorganized manner. The fostriecin arrested cells then progress into an aberrant form of anaphase. At the onset of “anaphase”, most fostriecin treated cells attempt chromosome separation in a tri- or poly-polar manner, which is associated with furrow ingression at three or more sites (shown at 5.3 hours in Figure 1B). In these cells, aberrant furrow ingression does not result in abscission. Rather, after a delay the furrows regress, producing a single tetraploid cell. Some cells reform three or more nuclei that are unequal in size (shown at 10.9 hr). Chromosome decondensation occurs prior to regression, and with time the tetraploid cells become apoptotic. By 48 hours, 50 μM fostriecin killed >98% of the cells, and the IC_{50} for 72 hr cytotoxic activity of fostriecin is ~5–7 μM (11, 17, 25). Only a small percentage (<4%) of the cells treated with 50 μM fostriecin become apoptotic prior the completion of mitosis (defined here as chromosome decondensation). Rather, in the majority of fostriecin treated cells, death occurred several

hours after furrow regression occurred (Figure 2B and 2D; black bars). The occasional cell that eventually achieves metaphase alignment was not killed and appeared to progress normally into anaphase. As reported previously for other cell types (13, 27) polyplody above 4N was not observed in fostriecin treated cells.

Suppression of PP4C prolongs mitosis and induces furrow regression prior to death

The concentration of fostriecin that altered mitotic progression is sufficient to completely inhibit the activity of PP2AC and PP4C, and the suppression of PP2AC did not produced furrow regression or tetraploid cells (29). Therefore, we developed antisense that specifically suppressed PP4C (Figure 1S). Antisense oligonucleotides targeting PP4C had no effect on the expression of PP2AC, PP5 or PP6C, and the level of these structurally related phosphatases do not increase to compensate for the lack of PP4C (Figure 3A). In the HeLa-H2B-GFP cell model, as observed in other cell lines, following treatment with antisense oligonucleotides targeting PP4C (PP4C-AS) >30 hours was required for PP4C protein levels to become maximally suppressed. Prior to ~50% suppression (~24 hours after treatment), cell division occurs normally. When PP4C levels are suppressed, PP4C-AS elicits a response that is strikingly similar to the response produced by fostriecin (compare Figures 1B and 1C). First, the suppression of PP4C produced no apparent differences from controls prior to NEBD. Second, treatment with 400 nM ISIS 134947 prolonged mitotic progression in ~60 % of the cells (4.33 hr +/− 0.47 hr; mean, SE, Fig. 2) compared to <4% in cells treated MM-controls. During this time, similar to the actions of fostriecin, cells arrested by PP4C-AS remain rounded in appearance and contained condensed chromosomes that fail to align properly at the metaphase plate (shown in Fig. 1C at 55 min and 2.5 hr). After a prolonged mitosis, multiple furrows initiate in the PP4-AS treated cells (shown at15 hr). With time the furrows regress and chromosomes undergo decondensation, resulting in a single tetraploid cell (shown at 18.2 hrs). However, it should be noted that when compared with fostriecin, both the average duration of mitosis and the time following furrow regression and proceeding apoptosis was highly variable in cells treated with PP4C-AS (compare bar length in Fig 2B and 2C). This difference may reflect difficulties associated with the uniform delivery of antisense-oligonucleotides to cell in culture, or may reflect the combined inhibition of both PP2AC and PP4C in the fostriecin treated cells. Additional data comparing the actions of fostriecin, PP4C-AS and PP2AC-AS is provided as supplemental data (Figures 2S & 3S).

Suppression of PP4C expression induces apoptosis in the absence of cellular stress

Initial dose-response studies (Figure 1E; Figure 1S) revealed that the suppression of PP4C kills HeLa cells in culture after 72 hrs (similar effects were observed in other lines of human cells). To determine if death induced by antisense oligonucleotides targeting PP4C is due to apoptosis, cells treated with ISIS 14376 or ISIS 134947 were examined. Light microscopic examination of dying cells revealed classic signs of apoptosis (i.e. membrane blebbing, and condensed fragmented DNA visualized by DAPI-staining). Electron microscopic analysis revealed numerous cells with homogenous condensation of chromatin contained in one side or the periphery of the nucleus in cells treated with antisense targeting PP4C, which is a hallmark characteristic of apoptosis (Figure 3E). Analysis of >100 cells 48 hours after treatment revealed condensed chromatin and other characteristics of apoptosis in 4% +/−1 of the cells treated with Lipofectin alone, 4% +/−2 of the cells treated with MM-control oligonucleotides (500 nM), 59% +/−3 of the cells treated with PP4C-AS at 300 nM, and 75%+/−8 of the cells treated PP4C-AS at 400 nM. Antisense oligonucleotides targeting PP4 also produced a dose-dependent increase in caspase 3 activity (Figure 3C). FACS analysis using an AnnexinV-FITC labeled antibody also revealed an increase in apoptosis when PP4C expression was suppressed (data not shown). These studies indicate that antisense

oligonucleotides capable of suppressing the expression of PP4C induce cell death via the induction of apoptosis.

Suppression of PP4C is associated with aberrant mitotic spindles

To explore mechanisms by which PP4C-AS may prolong mitosis, we examined the effects of ISIS 134947 on microtubule behavior. Immunostaining with fluorescent tagged anti-α-tubulin antibodies revealed that PP4C-AS has no apparent affect on microtubules in non-dividing cells (supplemental Figure 4S), while in mitotic cells marked differences were observed between the mismatch control- and PP4C-AS-treatment. At mitosis, > 98 % of the control cells contain a typical array of anti-parallel microtubules characteristic of a normal bipolar mitotic spindle. In contrast, in PP4C-AS treated cells the spindle apparatus was aberrant, often composed of multiple “poles” (Figure 4; indicated by arrows). Based on fluorescent immunostaining of fixed mitotic cells, it appears that PP4C-AS does not prevent the polymerization of microtubule structures in general. Rather, PP4C-AS disrupts the organization of the spindles.

Discussion

Microtubule binding drugs that disrupt mitotic progression (e.g. *Vinca* alkaloids and taxanes) have demonstrated efficacy in the treatment of different types of cancer. Accordingly, intense efforts have been devoted to further the understanding of how cancer cells responded to known anti-mitotic drugs and to the development of agents that perturb mitotic progression via other, less toxic, mechanisms. Indeed, agents targeting mitotic kinases [i.e. Polo-like kinase-1 (Plk1) and Aurora kinases] and microtubule associated motor proteins (e.g Eg5/Kinesin-5/KIF11 and CENP-E) are already in pre- or early-clinical development. The studies described here add support to the hypothesis that the inhibition of fostriecin sensitive phosphatases can also disrupt normal mitotic progression (Fig 1) without directly targeting microtubules, mitotic kinases or motor proteins (10, 27). Our data also provides new insight into the cytotoxic actions of fostriecin and reveal, for the first time, that the suppression of a little-studied fostriecin sensitive phosphatase (PP4C) is sufficient to prolong mitosis, alter cleavage furrow position/ingression, and induce apoptosis in the tetraploid cells produced following mitotic slippage.

Fostriecin is known to act as a strong inhibitor of PP2AC (10–12, 27), and fostriecin induces the accumulation of cells with 4N-DNA that have aberrant mitotic spindles prior to the onset of apoptosis (10, 13, 27). Therefore, when studies of PP2AC action during mitotic progression revealed that PP2AC (in a complex with PR61/B′ and Sgo1 at the kinetochore) functions to protect centromeric cohesion from phosphorylation-mediated dissociation by the activation of mitotic kinases (i.e. Plk-1 or Aurora B) (32, 33, 35), a simple hypothesis for the antitumor activity of fostriecin emerged. That is, the inhibition of PP2AC may allow the premature dissociation of centromeric cohesion (32–35), which prevents biorientation and triggers/maintains mitotic spindle assembly checkpoint controls. Studies with antisense oligonucleotides targeting PP2AC support this hypothesis, in the respect that the specific suppression of PP2ACα is sufficient to arrest cells in mitosis, and the PP2AC-AS arrested cells have lagging chromosomes that failed to align at the metaphase plate (29). Nonetheless, PP2AC can dephosphorylate a number of cyclinB-Cdk1 substrates (42(43), suggesting that the inhibition of PP2AC could also prolong mitosis via numerous other mechanisms.

A key novel observation reported here is that, although fostriecin treatment does prolong mitosis, apoptosis only occurs rarely during mitotic arrest (Figs. 1 and 2). This argues that fostriecin does not kill cells by simply prolonging mitosis. Further characterization revealed that the fostriecin treated cells exit mitosis (defined here as chromosome decondensation)

but then fail to complete cytokinesis. Death then occurs after mitotic slippage in the tetraploid cells that are produced, during what appears to be a second interphase. These novel actions of fostriecin are not observed following the suppression of PP1Cγ1, PP2ACα, PP2ACβ or PP5 (29–31), but are faithfully mimicked by the suppression of PP4C (Figs 1C, 2C).

Careful examination of the data reveals that there is great variation in the timing of cell death after treatment with fostriecin or antisense targeting PP4C. In general the actions of fostriecin were more uniform, which may reflect difficulties associated with various aspects of using antisense oligonucleotides in cultured cells (44), or differences produced by the rapid inhibition of PP4C activity by fostriecin compared to the gradual loss of PP4C protein following treatment with PP4-AS. Nonetheless, after treatment with either fostriecin or PP4-AS we observed no clear correlation between the duration of mitotic delay and cell fate, suggesting that in this cell model the time a cell spends in mitosis does not dictate if it dies in mitosis or slips from mitotic arrest and dies later after cleavage furrow regression.

Studies of PP4C function in human cells have revealed that it plays an important role in the recovery of cell cycle progression after DNA damage mediated S-phase arrest (45), which was not addressed by our experiments. However, investigations of PP4C function in lower organisms may provide insight into some of the other affects produced by antisense oligonucleotides targeting PP4C in HeLa cells. In *Drosophila* embryos, the PP4C orthologue (91% identical to human PP4C) is required for the organization of microtubules at the centrosomes (18), and siRNA mediated suppression in *Drosophila* affects polar division in neurons (46). The association of PP4C at the mitotic centrosomes has also been observed in higher organisms and is required for proper centrosome organization of microtubules (47, 48). Our studies show that the mitotic spindles in the PP4C-AS treated cells are aberrant (Figure 4), while the microtubules in non-mitotic cells appeared normal (supplemental data; Figure 4S). Although we can not rule out the possibility that PP4C plays an independent and non-redundant role to PP2AC in the regulation of centromeric cohesion, the appearance of miss-aligned and Y-shaped metaphase alignment of sister chromatids, produced by PP4C-AS or fostriecin (but not PP2AC-AS), would be an expected consequence of agents that disrupt normal microtubule attachment at the centrosomes. Presumably disruption of centrosome/microtubule interactions would also interfere with biorentation and prolong mitosis, which was observed after treatment with antisense specifically targeting PP4C.

Studies into the molecular mechanisms associated with cytokinetic abscission and signaling mechanism by which failures in cytokinesis can lead to regression and tetraploidy suggest reversible phosphorylation plays many regulatory roles. For example, in HeLa cells chromosome bridges sustain Aurora B activity, and Aurora B has been shown to protect missegregating cells against cleavage furrow regression via a mechanism in which Aurora B mediated phosphorylation of Mklp1 stabilizes Mklp1 at the intracellular canal (49). Chemical genetic studies of Plk1-function during mitosis indicate that the partial suppression of Plk1 can also result in cleavage furrow regression, leading to the formation of tetraploid cells (50). Phosphorylation at specific sites has been shown to activate Aurora B (Thr-232), Mlkp1 (Ser 911) and Plk1 (Thr-210). However, our data is not consistent with PP4C acting to directly dephosphorylate key activating sites on these kinases, because the inhibition of Aurora B, Plk1 or PP4C lead to furrow regression and the formation of tetraploid cells. Our data is consistent with PP4C playing an upstream role in which PP4C activity is needed to activate or maintain the activation of Aurora B or Plk1. Alternatively, PP4C could have indirect actions that affect a poorly characterized aspect of these known pathways. Clearly future studies will be required to determine the molecular mechanisms by which the suppression of PP4C produces mitotic slippage and tetraploid cell death.

Supplementary Material

Refer to Web version on PubMed Central for supplementary material.

Acknowledgments

This work was supported in part by the University of South Alabama Cancer Research Fund, an intramural grant program funded by the USA Mitchell Cancer Institute, the National Institutes of Health (NCI grant CA-60750 to REH) and the National Science Foundation (NSF 0751684). This investigation use equipment purchased with funds from a shared instrument grant (S10RR027535) and was conducted in a facility constructed with support from Research Facilities Improvement Program Grant (C06 RR11174) from the National Center for Research Resources.

References

1. Lewy DS, Gauss CM, Soenen DR, Boger DL. Fostriecin: chemistry and biology. Curr Med Chem. 2002 Nov; 9(22):2005–32. [PubMed: 12369868]
2. Honkanen RE, Golden T. Regulators of serine/threonine protein phosphatases at the dawn of a clinical era? Curr Med Chem. 2002 Nov; 9(22):2055–75. [PubMed: 12369870]
3. Kawada M, Amemiya M, Ishizuka M, Takeuchi T. Differential induction of apoptosis in B16 melanoma and EL-4 lymphoma cells by cytostatin and bactobolin. Jpn J Cancer Res. 1999 Feb; 90(2):219–25. [PubMed: 10189893]
4. Leopold WR, Shillis JL, Mertus AE, Nelson JM, Roberts BJ, Jackson RC. Anticancer activity of the structurally novel antibiotic Cl-920 and its analogues. Cancer Res. 1984 May; 44(5):1928–32. [PubMed: 6546897]
5. de Jong RS, de Vries EG, Mulder NH. Fostriecin: a review of the preclinical data. Anticancer Drugs. 1997 Jun; 8(5):413–8. [PubMed: 9215602]
6. Honkanen RE. Serine/threonine protein phosphatase inhibitors with anti tumor activity. Handbook of Exp Pharm. 2005; 167:295–317.
7. Le LH, Erlichman C, Pillon L, et al. Phase I and pharmacokinetic study of fostriecin given as an intravenous bolus daily for five consecutive days. Invest New Drugs. 2004 Apr; 22(2):159–67. [PubMed: 14739664]
8. de Jong RS, Mulder NH, Uges DR, et al. Phase I and pharmacokinetic study of the topoisomerase II catalytic inhibitor fostriecin. Br J Cancer. 1999 Feb; 79(5–6):882–7. [PubMed: 10070885]
9. Susick RL Jr, Hawkins KL, Pegg DG. Preclinical toxicological evaluation of fostriecin, a novel anticancer antibiotic, in rats. Fundam Appl Toxicol. 1990 Aug; 15(2):258–69. [PubMed: 2227154]
10. Walsh AH, Cheng A, Honkanen RE. Fostriecin, an antitumor antibiotic with inhibitory activity against serine/threonine protein phosphatases types 1 (PP1) and 2A (PP2A), is highly selective for PP2A. FEBS Lett. 1997 Oct 27; 416(3):230–4. [PubMed: 9373158]
11. Buck SB, Hardouin C, Ichikawa S, et al. Fundamental role of the fostriecin unsaturated lactone and implications for selective protein phosphatase inhibition. J Am Chem Soc. 2003 Dec 24; 125(51): 15694–5. [PubMed: 14677930]
12. Swingle MR, Amable L, Lawhorn BG, et al. Structure-activity relationship studies of fostriecin, cytostatin, and key analogs, with PP1, PP2A, PP5, and (beta12-beta13)-chimeras (PP1/PP2A and PP5/PP2A), provide further insight into the inhibitory actions of fostriecin family inhibitors. J Pharmacol Exp Ther. 2009 Oct; 331(1):45–53. [PubMed: 19592665]
13. Roberge M, Tudan C, Hung SM, Harder KW, Jirik FR, Anderson H. Antitumor drug fostriecin inhibits the mitotic entry checkpoint and protein phosphatases 1 and 2A. Cancer Res. 1994 Dec 1; 54(23):6115–21. [PubMed: 7954457]
14. Kawada M, Amemiya M, Ishizuka M, Takeuchi T. Cytostatin, an inhibitor of cell adhesion to extracellular matrix, selectively inhibits protein phosphatase 2A. Biochim Biophys Acta. 1999 Nov 11; 1452(2):209–17. [PubMed: 10559474]
15. Lawhorn BG, Boga SB, Wolkenberg SE, et al. Total synthesis and evaluation of cytostatin, its C10-C11 diastereomers, and additional key analogues: impact on PP2A inhibition. J Am Chem Soc. 2006 Dec 27; 128(51):16720–32. [PubMed: 17177422]

16. Usui T, Marriott G, Inagaki M, Swarup G, Osada H. Protein phosphatase 2A inhibitors, phoslactomycins. Effects on the cytoskeleton in NIH/3T3 cells. J Biochem. 1999 May; 125(5): 960–5. [PubMed: 10220590]

17. Swingle M, Ni L, Honkanen RE. Small-molecule inhibitors of ser/thr protein phosphatases: specificity, use and common forms of abuse. Methods Mol Biol. 2007; 365:23–38. [PubMed: 17200551]

18. Hastie CJ, Cohen PT. Purification of protein phosphatase 4 catalytic subunit: inhibition by the antitumour drug fostriecin and other tumour suppressors and promoters. FEBS Lett. 1998 Jul 24; 431(3):357–61. [PubMed: 9714542]

19. Swingle MR, Honkanen RE, Ciszak EM. Structural basis for the catalytic activity of human serine/threonine protein phosphatase-5. J Biol Chem. 2004 Aug 6; 279(32):33992–9. [PubMed: 15155720]

20. Takeuchi T, Takahashi N, Ishi K, Kusayanagi T, Kuramochi K, Sugawara F. Antitumor antibiotic fostriecin covalently binds to cysteine-269 residue of protein phosphatase 2A catalytic subunit in mammalian cells. Bioorg Med Chem. 2009 Dec 1; 17(23):8113–22. [PubMed: 19857968]

21. Gao D, O'Doherty GA. Total synthesis of fostriecin: via a regio- and stereoselective polyene hydration, oxidation, and hydroboration sequence. Org Lett. Sep 3; 12(17):3752–5. [PubMed: 20687585]

22. Hayashi Y, Yamaguchi H, Toyoshima M, Okado K, Toyo T, Shoji M. Formal total synthesis of fostriecin by 1,4-asymmetric induction with an alkyne-cobalt complex. Chemistry. Sep 3; 16(33): 10150–9. [PubMed: 20645347]

23. Fry DW, Besserer JA, Boritzki TJ. Transport of the antitumor antibiotic Cl-920 into L1210 leukemia cells by the reduced folate carrier system. Cancer Res. 1984 Aug; 44(8):3366–70. [PubMed: 6547636]

24. Spinella MJ, Brigle KE, Sierra EE, Goldman ID. Distinguishing between folate receptor-alpha-mediated transport and reduced folate carrier-mediated transport in L1210 leukemia cells. J Biol Chem. 1995 Apr 7; 270(14):7842–9. [PubMed: 7713875]

25. Pillon L, Moore MJ, Thiessen JJ. Determination of fostriecin pharmacokinetics in plasma using high-pressure liquid chromatography assay. Ther Drug Monit. 1994 Apr; 16(2):186–90. [PubMed: 8009568]

26. Hotz MA, Traganos F, Darzynkiewicz Z. Changes in nuclear chromatin related to apoptosis or necrosis induced by the DNA topoisomerase II inhibitor fostriecin in MOLT-4 and HL-60 cells are revealed by altered DNA sensitivity to denaturation. Exp Cell Res. 1992 Jul; 201(1):184–91. [PubMed: 1319346]

27. Cheng A, Balczon R, Zuo Z, Koons JS, Walsh AH, Honkanen RE. Fostriecin-mediated G2-M-phase growth arrest correlates with abnormal centrosome replication, the formation of aberrant mitotic spindles, and the inhibition of serine/threonine protein phosphatase activity. Cancer Res. 1998 Aug 15; 58(16):3611–9. [PubMed: 9721869]

28. Boritzki TJ, Wolfard TS, Besserer JA, Jackson RC, Fry DW. Inhibition of type II topoisomerase by fostriecin. Biochem Pharmacol. 1988 Nov 1; 37(21):4063–8. [PubMed: 2847752]

29. Bonness K, Aragon IV, Rutland B, Ofori-Acquah S, Dean NM, Honkanen RE. Cantharidin-induced mitotic arrest is associated with the formation of aberrant mitotic spindles and lagging chromosomes resulting, in part, from the suppression of PP2Aalpha. Mol Cancer Ther. 2006 Nov; 5(11):2727–36. [PubMed: 17121919]

30. Zuo Z, Dean NM, Honkanen RE. Serine/threonine protein phosphatase type 5 acts upstream of p53 to regulate the induction of p21(WAF1/Cip1) and mediate growth arrest. J Biol Chem. 1998 May 15; 273(20):12250–8. [PubMed: 9575175]

31. Cheng A, Dean NM, Honkanen RE. Serine/threonine protein phosphatase type 1gamma1 is required for the completion of cytokinesis in human A549 lung carcinoma cells. J Biol Chem. 2000 Jan 21; 275(3):1846–54. [PubMed: 10636884]

32. Tang Z, Shu H, Qi W, Mahmood NA, Mumby MC, Yu H. PP2A is required for centromeric localization of Sgo1 and proper chromosome segregation. Dev Cell. 2006 May; 10(5):575–85. [PubMed: 16580887]

33. Riedel CG, Katis VL, Katou Y, et al. Protein phosphatase 2A protects centromeric sister chromatid cohesion during meiosis I. Nature. 2006 May 4; 441(7089):53–61. [PubMed: 16541024]
34. Watanabe Y, Kitajima TS. Shugoshin protects cohesin complexes at centromeres. Philos Trans R Soc Lond B Biol Sci. 2005 Mar 29; 360(1455):515–21. discussion 21. [PubMed: 15897177]
35. Xu Z, Cetin B, Anger M, et al. Structure and function of the PP2A-shugoshin interaction. Mol Cell. 2009 Aug 28; 35(4):426–41. [PubMed: 19716788]
36. Kanda T, Sullivan KF, Wahl GM. Histone-GFP fusion protein enables sensitive analysis of chromosome dynamics in living mammalian cells. Curr Biol. 1998 Mar 26; 8(7):377–85. [PubMed: 9545195]
37. Dean NM, Griffey RH. Identification and characterization of second-generation antisense oligonucleotides. Antisense Nucleic Acid Drug Dev. 1997 Jun; 7(3):229–33. [PubMed: 9212916]
38. Urban G, Golden T, Aragon IV, et al. Identification of a functional link for the p53 tumor suppressor protein in dexamethasone-induced growth suppression. J Biol Chem. 2003 Mar 14; 278(11):9747–53. [PubMed: 12519780]
39. Huang X, Cheng A, Honkanen RE. Genomic organization of the human PP4 gene encoding a serine/threonine protein phosphatase (PP4) suggests a common ancestry with PP2A. Genomics. 1997 Sep 15; 44(3):336–43. [PubMed: 9325055]
40. Zuo Z, Urban G, Scammell JG, et al. Ser/Thr protein phosphatase type 5 (PP5) is a negative regulator of glucocorticoid receptor-mediated growth arrest. Biochemistry. 1999 Jul 13; 38(28): 8849–57. [PubMed: 10413457]
41. Kloeker S, Reed R, McConnell JL, et al. Parallel purification of three catalytic subunits of the protein serine/threonine phosphatase 2A family (PP2A(C), PP4(C), and PP6(C)) and analysis of the interaction of PP2A(C) with alpha4 protein. Protein Expr Purif. 2003 Sep; 31(1):19–33. [PubMed: 12963337]
42. Forester CM, Maddox J, Louis JV, Goris J, Virshup DM. Control of mitotic exit by PP2A regulation of Cdc25C and Cdk1. Proc Natl Acad Sci U S A. 2007 Dec 11; 104(50):19867–72. [PubMed: 18056802]
43. Burgess A, Vigneron S, Brioudes E, Labbe JC, Lorca T, Castro A. Loss of human Greatwall results in G2 arrest and multiple mitotic defects due to deregulation of the cyclin B-Cdc2/PP2A balance. Proc Natl Acad Sci U S A. Jul 13; 107(28):12564–9. [PubMed: 20538976]
44. Honkanen, RE. Serine Threonine Protein Phosphatases. In: Crooke, ST., editor. Antisense Drug Technology: Principles, Strategies, and Applications. Marcel Dekker, Inc; New York: 2001. p. 587-614.
45. Chowdhury D, Xu X, Zhong X, et al. A PP4-phosphatase complex dephosphorylates gamma-H2AX generated during DNA replication. Mol Cell. 2008 Jul 11; 31(1):33–46. [PubMed: 18614045]
46. Sousa-Nunes R, Chia W, Somers WG. Protein phosphatase 4 mediates localization of the Miranda complex during Drosophila neuroblast asymmetric divisions. Genes Dev. 2009 Feb 1; 23(3):359–72. [PubMed: 19204120]
47. Toyo-oka K, Mori D, Yano Y, et al. Protein phosphatase 4 catalytic subunit regulates Cdk1 activity and microtubule organization via NDEL1 dephosphorylation. J Cell Biol. 2008 Mar 24; 180(6): 1133–47. [PubMed: 18347064]
48. Ou Y, Rattner JB. The centrosome in higher organisms: structure, composition, and duplication. Int Rev Cytol. 2004; 238:119–82. [PubMed: 15364198]
49. Steigemann P, Wurzenberger C, Schmitz MH, et al. Aurora B-mediated abscission checkpoint protects against tetraploidization. Cell. 2009 Feb 6; 136(3):473–84. [PubMed: 19203582]
50. Lera RF, Burkard ME. High mitotic activity of Polo-like kinase 1 is required for chromosome segregation and genomic integrity in human epithelial cells. J Biol Chem. Dec 14; 287(51):42812–25. [PubMed: 23105120]

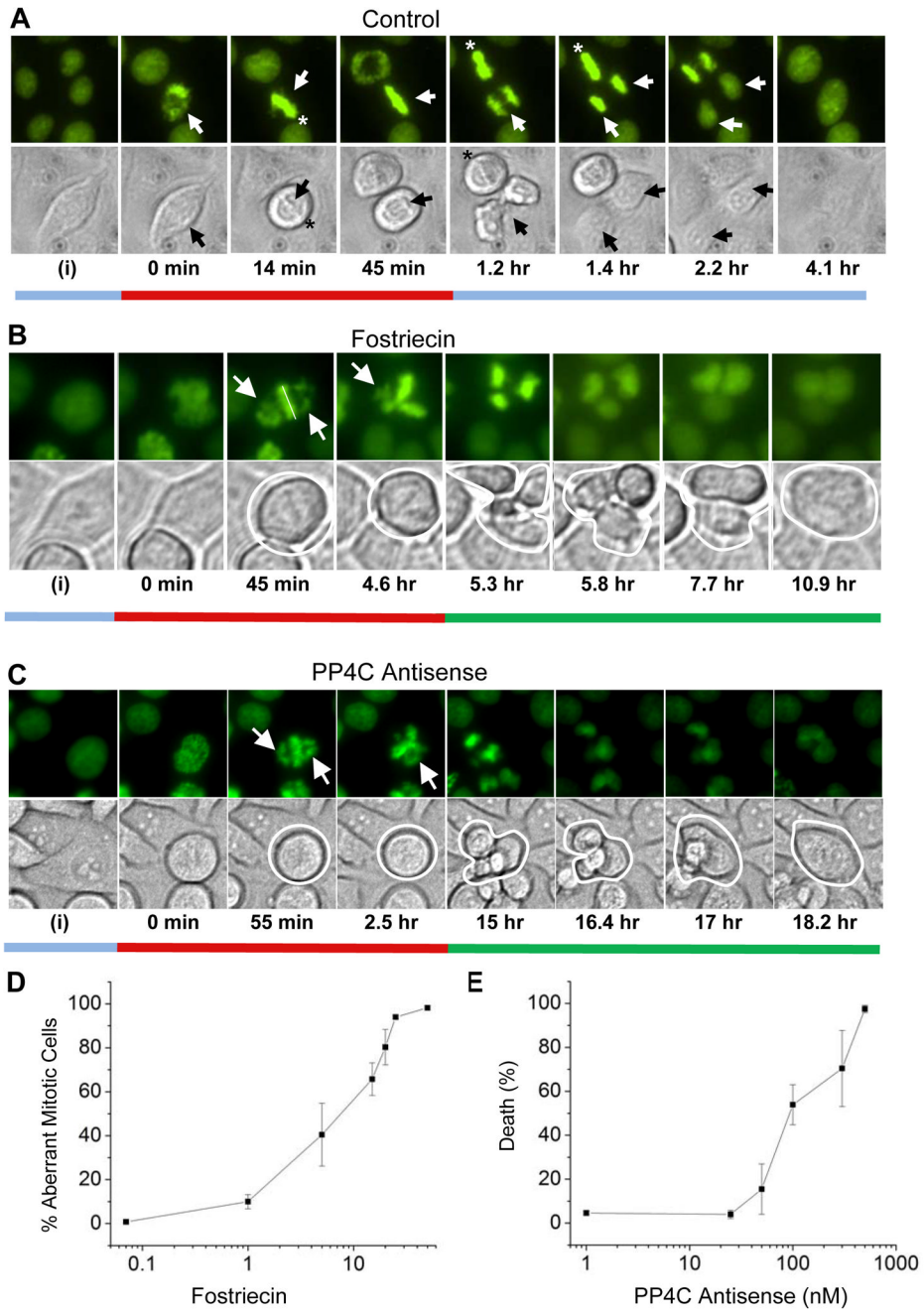

Figure 1. Localization of H2B-GFP protein in HeLa cells

Fluorescent and corresponding differential interference contrast (DIC) microscopic images of selected HeLa-H2B-GFP cells representing the typical behavior of the populations are shown at various phases of the cell cycle. A) Representative images selected from time-lapse live cell imaging of control cells typical of: interphase at the start of recording (i), the start of mitotic entry (set at 0 min), pro-metaphase (14 min), metaphase (45 min), anaphase (1.2–1.4 hr), chromosome decondensation (2.2 hr) and after the completion of cytokinesis (4.1 hr). Elapsed time from the start of mitotic entry is indicated below image pairs. B) Images showing selected cells that represent the typical behavior of populations after treatment with 50 μM fostriecin. No effects were observed prior to entry into mitosis (0

min). During a prolonged mitosis, condensed chromosomes fail to align properly at the metaphase plate (45 min; 4.6 hr). Subsequently, chromosomes segregated into unequal clusters (5.3 hr) and undergo decondensation (5.8 hr). During this period more than one furrow appears (5.3 hr; 5.8 hr and 7.7 hr). Then the furrows undergo regression (shown here at 10.9 hrs). C) Images showing selected cells that represent the typical behavior of populations after treatment with antisense oligonucleotides targeting PP4C. H2B-GFP expressing HeLa cells were treated with 400 nM ISIS 134947. After 24 hours, time-lapse imaging studies were conducted for 48 hours as above. The similarity to the effects produced by fostriecin are striking: PP4C-AS interferes with the integrity of the metaphase plate (55 min) prolongs mitosis, and allows cleavage furrow regression following mitotic slippage (shown at 18.2 hr). The data shown is representative of > 4 separate experiments in which 50–100 mitotic cells were scored in each experiment. Bars under figure pairs are colored to illustrate images representing various stages of cell cycle progression and are color matched to the quantitative data shown in Figure 2. D) Concentration dependent increase in fostriecin-mediated failure of chromosome alignment at the metaphase plate. HeLa-H2B-GFP cells were treated with the indicated concentration of fostriecin or solvent (controls). After 24 hours fluorescent images of random fields were taken, and 50–100 mitotic cells were examined for the presence of condensed chromosomes that failed to align properly at the metaphase plate. The data shown represent the mean +/− SD from three separate experiments. E) Dose-dependent cell death following treatment with antisense targeting PP4C. HeLa cells were treated with the indicated concentration of ISIS 14376, and cell viability was determined after 72 hours. For each experiment random fields were examined and 100 cells were scored for by the ability to exclude trypan blue. The data is plotted as death (%) as compared to death in cells treated with miss-matched antisense oligonucleotides and represents the mean +/− SD (n=3).

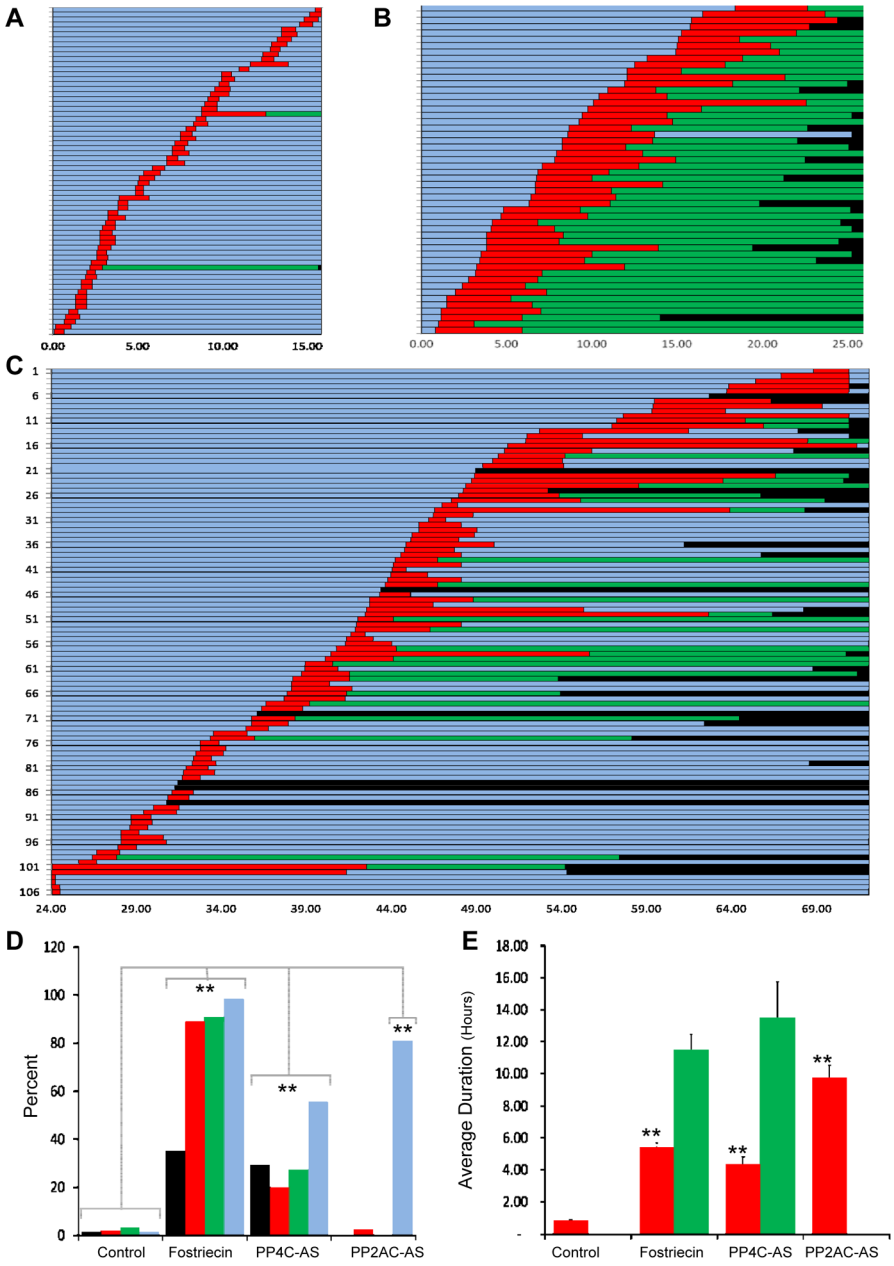

Figure 2. Quantification of data obtained from images taken during experiments, as shown in Figure 1

The duration and fate of 50–100 cells entering mitosis in each experiment was recorded. The plot depicts the duration of mitosis and fate of the cells from a single representative experiment. Each horizontal bar represents a single cell, and the color of the bar denotes the fate of the cell. Blue bars represent time spent in interphase. Red bars represent the time spent in mitosis (defined by the time from NEBD to anaphase onset), green bars indicate cells in which cytokinesis fails (producing tetraploid cells that then enter into a second interphase). Black bars indicate death. The length of the bars (excluding black bars; death) denotes the duration of each fate, and the scale below the graph shows time in hours. A) Controls. B) Cells treated with 50 μM fostriecin, C) Cells treated with PP4-AS as described in Figure 1. D) Bar graph representation of the percentage of cells that: die following mitosis

(black), undergo cleavage furrow regression (green); undergo mitotic slippage and reform >2 daughter nuclei of unequal size (red); and arrest in mitosis for >2.5 hours (blue). ** indicates a difference from controls ($p<0.01$) for bracketed values determined by two tailed t-test. E) Bar graph comparing the average duration of mitosis (red) and the average time spent in the second apparent interphase (green; identified by cleavage furrow regression and chromosome decondensation) and preceding death. ** indicates a difference from controls ($p<0.01$) according to independent t-tests between means.

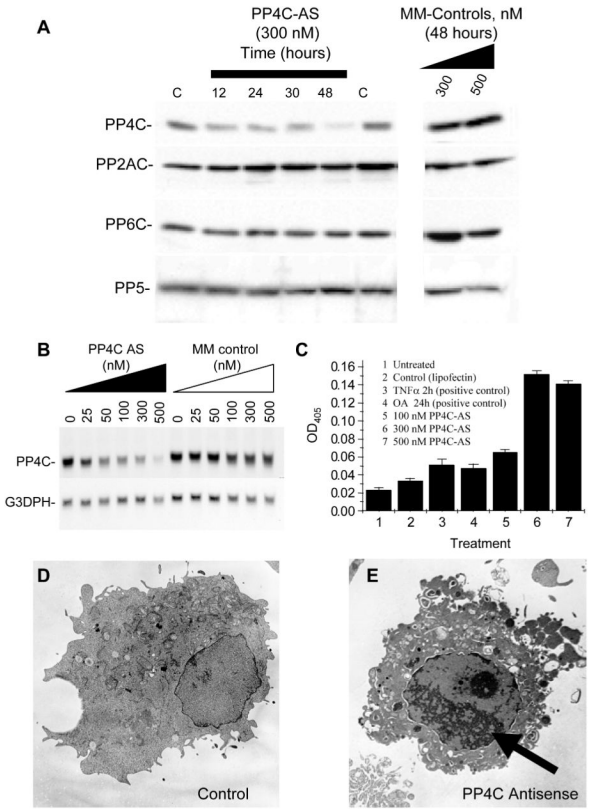

Figure 3. Affects of antisense oligodoexynucleotides targeting PP4C

A) Target specific inhibition of PP4C protein levels. Cells were treated with the either antisense oligonucleotides targeting PP4C (ISIS 134947 illustrated) or mismatch control oligonucleotides (MM; ISIS 131370 or ISIS 131371). Protein extracts were prepared at the times indicated and analyzed for structurally related phosphatases (PP2AC, PP4C, PP5 and PP6C) by western blot analysis as described in Methods [the antibody for PP2AC recognizes both the α and β isoforms of PP2AC (29)]. B) Dose-dependent suppression of PP4C mRNA levels by ISIS 134947 in HeLa cells. To ensure the uptake and efficacy of antisense oligonucleotides, for each experiment replicate plates were treated with the oligonucleotides indicated and processed for Northern analysis after 24 hours, as described in Figure 1S and supplemental methods. Representative data obtained using ISIS 134947 and MM (ISIS 131371) are shown. C) Caspase 3 activity. A549 cells were treated with nothing (1), lipofectin (lipid control; 2), 10 nM TNFα (positive control;3), 10 nM okadaic acid (OA; second positive control;4), or the indicated concentration of ISIS 14376 (PP4C-AS; 5,6,7). After 36 hours, cells were harvested and caspase-3 activity was measured as described in methods. The data is plotted as the mean OD_{405} +/− SE from three replicate plates, and is representative of three separate experiments. D and E) Representative electron micrographs of A549 cell populations after treatment with MM (control) or antisense oligonucleotides (ISIS 14376) targeting PP4C. After treatment (48 hours) cells were harvested, fixed, stained and then viewed by electron microscopy using standard protocols. Controls (D) have an intact membrane, organelles, and normal nuclear morphology. ISIS 14376 treated cells (E) show homogeneous chromatin condensation within the nucleus (arrow), membrane blebbing and other characteristics common to apoptotic cells.

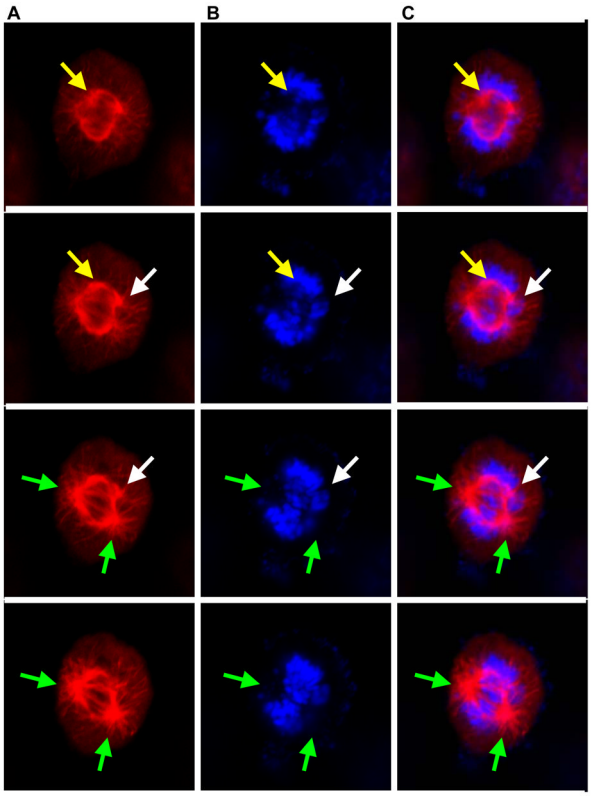

Figure 4. Mitotic abnormalities associated with the suppression of PP4C

Representative confocal microscopic images of serial Z sections through a HeLa cell treated with antisense targeting PP4C. Cells were treated with 400 nM ISIS 134947 and fixed on cover slips 30 hours later. A) Microtubules (red) were then visualized by immunofluorescence following treatment with anti-α-tubulin and Alexa-Fluor 594-labeled antibodies as described in Methods. B) DNA (blue) was visualized by staining with Hoechst 33342. C) Computer assisted merge of images A and B. Similar results were obtained with ≥ 3 independent experiments.